J Med Syst (2016) 40: 106
DOI 10.1007/s10916-016-0450-4

EDUCATION & TRAINING

Computational Diffusion Magnetic Resonance Imaging Based on Time-Dependent Bloch NMR Flow Equation and Bessel Functions

Bamidele O. Awojoyogbe[1] · **Michael O. Dada**[1] · **Samuel O. Onwu**[1] · **Taofeeq A. Ige**[2] · **Ninuola I. Akinwande**[3]

Received: 12 June 2014 / Accepted: 26 January 2016 / Published online: 18 February 2016

Abstract Magnetic resonance imaging (MRI) uses a powerful magnetic field along with radio waves and a computer to produce highly detailed "slice-by-slice" pictures of virtually all internal structures of matter. The results enable physicians to examine parts of the body in minute detail and identify diseases in ways that are not possible with other techniques. For example, MRI is one of the few imaging tools that can see through bones, making it an excellent tool for examining the brain and other soft tissues. Pulsed-field gradient experiments provide a straightforward means of obtaining information on the translational motion of nuclear spins. However, the interpretation of the data is complicated by the effects of restricting geometries as in the case of most cancerous tissues and the mathematical concept required to account for this becomes very difficult. Most diffusion magnetic resonance techniques are based on the Stejskal-Tanner formulation usually derived from the Bloch-Torrey partial differential equation by including additional terms to accommodate the diffusion effect. Despite the early success of this technique, it has been shown that it has important limitations, the most of which occurs when there is orientation *heterogeneity* of the fibers in the voxel of interest (VOI). Overcoming this difficulty requires the specification of diffusion coefficients as function of spatial coordinate(s) and such a phenomenon is an indication of non-uniform compartmental conditions which can be analyzed accurately by solving the time-dependent Bloch NMR flow equation analytically. In this study, a mathematical formulation of magnetic resonance flow sequence in restricted geometry is developed based on a general second order partial differential equation derived directly from the fundamental Bloch NMR flow equations. The NMR signal is obtained completely in terms of NMR experimental parameters. The process is described based on Bessel functions and properties that can make it possible to distinguish cancerous cells from normal cells. A typical example of liver distinguished from gray matter, white matter and kidney is demonstrated. Bessel functions and properties are specifically needed to show the direct effect of the instantaneous velocity on the NMR signal originating from normal and abnormal tissues.

Keywords Bloch NMR flow equations · NMR advection-diffusion equation · Brain tumor · Gray matter · White matter · Cerebrospinal fluid · Bessel functions · Sickle cell disease · Cancerous tissues · Phase shift

This article is part of the Topical Collection on *Education & Training*

✉ Bamidele O. Awojoyogbe
awojoyogbe@yahoo.com

[1] Department of Physics, Federal University of Technology, P.M.B. 65, Minna, Niger State, Nigeria

[2] Department of Medical Physics, National Hospital, P.M.B. 425, Abuja, Nigeria

[3] Department of Pure and Applied Mathematics, Federal University of Technology, P.M.B. 65, Minna, Niger State, Nigeria

Introduction

Magnetic Resonance Angiography (MRA) is a group of techniques based on Magnetic Resonance Imaging (MRI) to image blood vessels [1]. MRA is used to generate images of the arteries in order to evaluate them for stenosis (abnormal narrowing of blood vessels), occlusion or aneurysms. MRA has been successful in studying many arteries in the body, including cerebral and other vessels in the head and neck, the aorta and its major branches in the thorax and abdomen, the renal arteries, and the arteries in the lower limbs. For the

Table 1 Diffusion and NMR relaxation parameters of different tissues

Tissues	ADC (m^2/s)	T_2 (s)	T_1 (s)	T_0 (s^{-1})	T_g (s^{-2})	ζ	β^2	p	n
White brain matter	7.00E-10	0.070	0.66	15.80087	21.64502	–21.8189	0.061181	–0.77837	0.738024
Gray brain matter	8.90E-10	0.088	0.76	12.67943	14.95215	–27.7412	0.173114	–0.92803	0.829534
Liver	1.83E-09	0.029	0.39	37.04686	88.41733	–57.0409	0.491559	–1.27035	1.059354
Kidney	2.19E-09	0.034	0.47	31.53942	62.57822	–68.2621	1.027738	–1.54985	1.172301

coronary arteries, however, MRA has been less successful than CT angiography or invasive catheter angiography. Most often, the underlying disease is atherosclerosis, but medical conditions like aneurysms or abnormal vascular anatomy can also be diagnosed.

An advantage of MRA compared to invasive catheter angiography is the non-invasive character of the examination. Another advantage, compared to CT angiography and catheter angiography, is that the patient is not exposed to any ionizing radiation. Also, contrast media used for MRI tend to be less toxic than those used for CT angiography and catheter angiography. The greatest drawbacks of the method are its comparatively high cost and its somewhat limited spatial resolution [1].In order to address this problem, multi-modal imaging techniques are employed. The use of diffusion imaging with MRA has been quite successful in this multi-modal method.

Traditionally diffusion weighted MRI involves two gradient pulses [1–13]. The first gradient pulse will impart a spatially-dependent phase to each excited spin. For stationary spins, the second gradient phase will reverse the phase introduced by the first gradient pulse and hence the bipolar gradient will have no net effect. There will be a phase offset proportional to the distance travelled, for spins that are displaced between the applications of the two gradient pulses. This phase dispersion, in turn, attenuates the signal exponentially

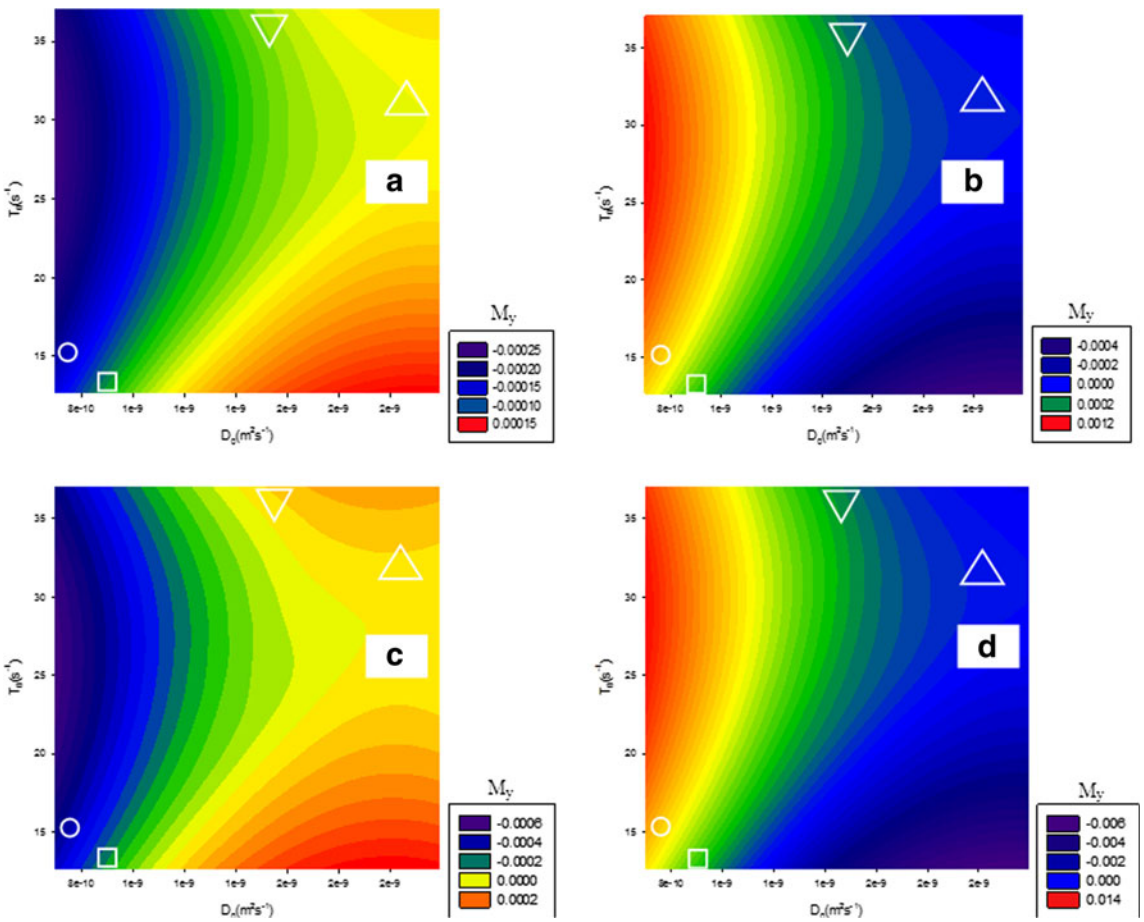

Fig. 1 Contour maps of $\frac{M_y}{A}$ as a funcion of relaxation rate T_0 and ADC (D_0) for (**a**) x = 0.005m (**b**) x = 0.0005m (**c**) x = 0.00005m (**d**) x = 0.000005m. The marked regions on the map correspond to different tissues: O- white matter, □ - gray matter, ∇- liver, Δ- kidney

according to the b-factor and the diffusion coefficient (D; a measure of the strength (velocity) of diffusion in tissue).

For unrestricted flow the generalized magnetic resonance mathematical framework [2, 13] relating the signal attenuation, $\frac{S}{S_0}$; the conditional displacement distribution, the pulse duration, δ; the pulse strength, g; the gyromagnetic ratio, γ; results in a Gaussian distribution of the form

$$A = \frac{S}{S_0} = e^{-bD} \tag{1}$$

where S_0 is the signal intensity without diffusion weighting. S is the diffusion weighted signal. The b-value identifies the measurement's sensitivity to diffusion and determines the strength and duration of the diffusion gradients and is measured in s/mm^2 (1–10).

$$b = \gamma^2 g^2 \delta^2 \left(\Delta - {}^{\delta}/_{3} \right) \tag{2}$$

where g is the amplitude of the two diffusion gradient pulses, and Δ is the time between two pulses.

DW-MRI is useful in the diagnosis and monitoring of a number of neurological diseases such as cancer, multiple

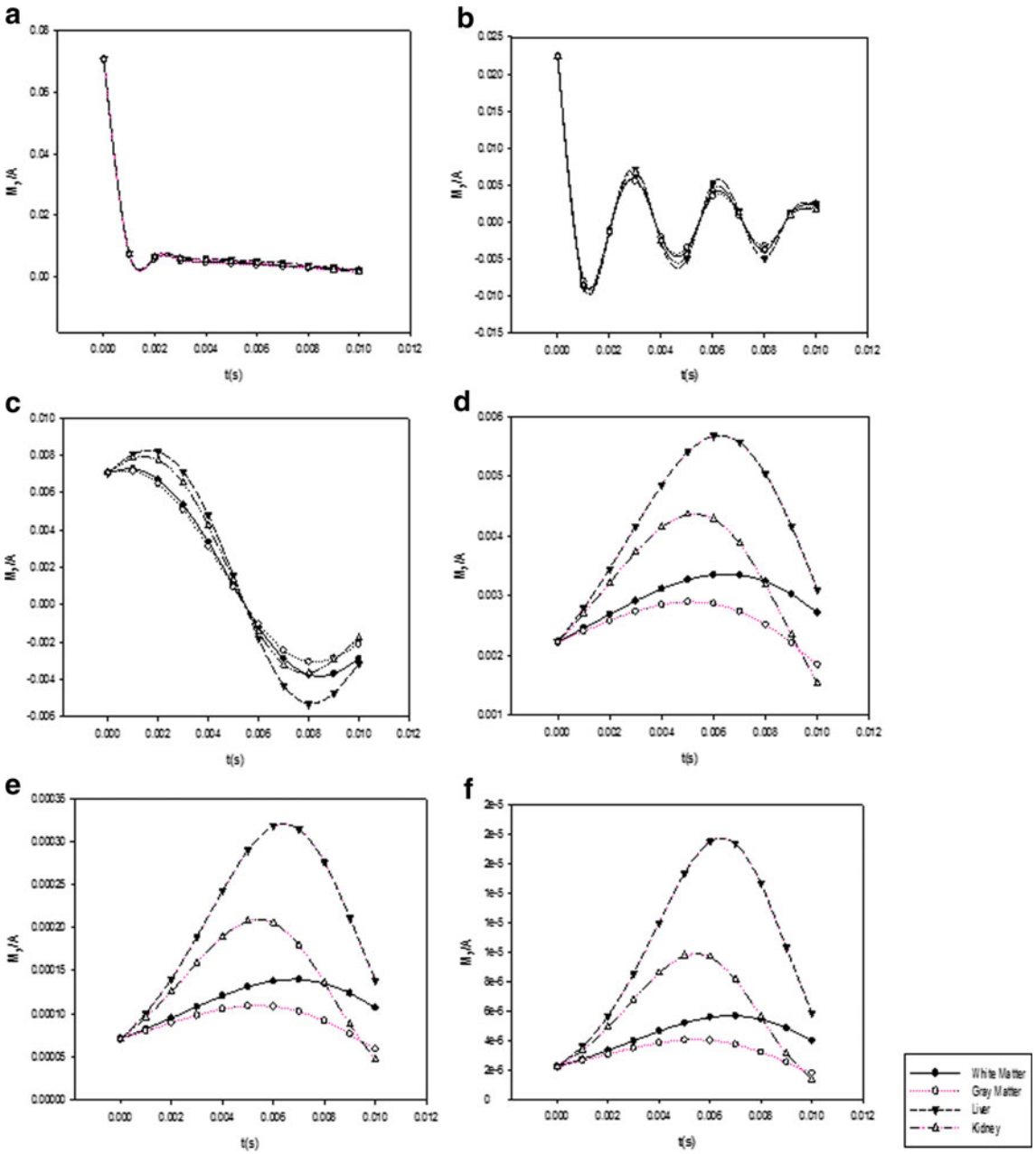

Fig. 2 Plots of $\frac{M_y}{A}$ against t (= δ) for different tissues at (**a**) x = 0.005m (**b**) x = 0.0005m (**c**) x = 0.00005m (**d**) x = 5μm (**e**) x = 5nm (**f**) x = 5pm

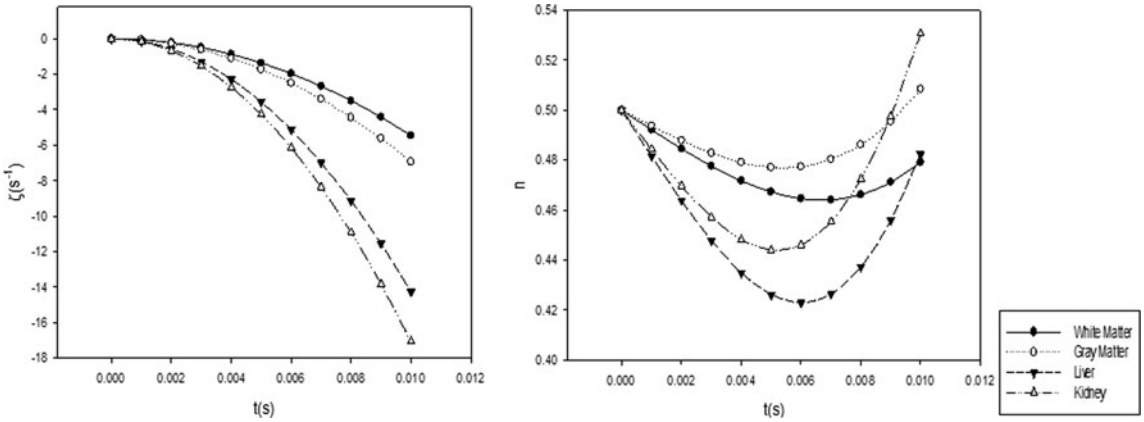

Fig. 3 Plots of NMR parameters ξ and n against t (= δ) for different tissues

sclerosis and Alzheimer. The most profound clinical impact of diffusion contrast has been in the diagnosis of acute stroke. Diffusion imaging is extremely sensitive to motion artifacts; hence, motion correction is a vital component of any in vivo multi-shot DWI pulse sequence [1–4].

The simple expression in equation (2) highlights how variations in the spatial scale parameter, b, and the diffusion time, Δ, independently affect the signal attenuation. In a medium in which water does not move freely but confined within internal compartments (restricted) or

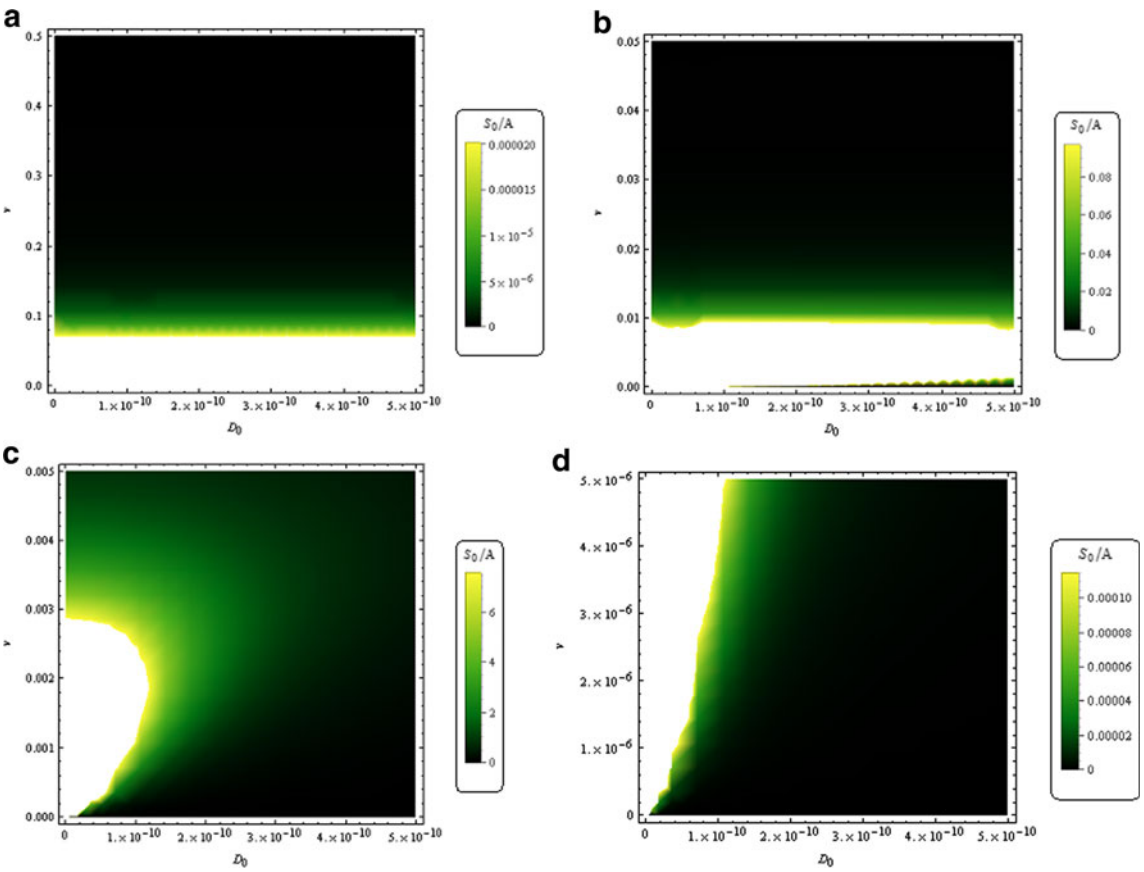

Fig. 4 Density plots of $\frac{S_0}{A}$ against v and D_0 for $u_0 = 44138 m^{-1}$ ($g = 33 mTm^{-1}$, $\delta = 20 ms$), $p = -1$, $n = 0$. Different ranges of velocities are considered

experiences higher diffusivity in some directions and lower in others (anisotropic) the simple relationship in equation (2) no longer holds [3–9, 13].

In this investigation, we shall apply the one dimensional NMR equation where we derived analytical expressions for the NMR transverse magnetization [10–26] which can be detected by the recovery unit in the MRI scanner based on the Bloch NMR flow equations with the assumption that resonance condition exists at Larmor frequency [23–25]:

$$f_o = \gamma B - \omega = 0$$

The x, y, z components (in the rotating frame) of the magnetization of a particle may be given by the Bloch NMR flow equations which may be written as follows [25]:

$$\frac{dM_x}{dt} = \frac{\partial M_x}{\partial t} + v \cdot \nabla M_x = -\frac{M_x}{T_2} \tag{3a}$$

$$\frac{dM_y}{dt} = \frac{\partial M_y}{\partial t} + v \cdot \nabla M_y = \gamma M_z B_1(x) - \frac{M_y}{T_2} \tag{3b}$$

$$\frac{dM_z}{dt} = \frac{\partial M_z}{\partial t} + v \cdot \nabla M_z = \gamma M_z B_1(x) - \frac{M_o - M_z}{T_1} \tag{3c}$$

From equations (3b and 3c), we obtained the following second order time dependent differential equation which can be solved analytically in Cartesian, Cylindrical and Spherical geometries [11–26].

$$v^2 \frac{\partial^2 M_y}{\partial x^2} + 2v \frac{\partial^2 M_y}{\partial x \partial t} + \frac{\partial^2 M_y}{\partial t^2} + \left(\frac{1}{T_1} + \frac{1}{T_2}\right) v \frac{\partial M_y}{\partial x} + \left(\frac{1}{T_1} + \frac{1}{T_2}\right) \frac{\partial M_y}{\partial t} + \left(\gamma^2 B_1{}^2(t) + \frac{1}{T_1 T_2}\right) M_y = \frac{M_o \gamma B_1(x,t)}{T_1} \tag{4}$$

where γ is the gyromagnetic ratio of the fluid particle. The solution presented here is subject to the following two reasonable initial boundary conditions which may conform to the real-time experimental arrangements:

1. $M_o \neq M_z$, a situation which hold good in general and in particular when the RF $B_1(t)$ field is strong.
2. Before entering signal detector coil, the soft particle has $M_x = 0$, $M_y = 0$.

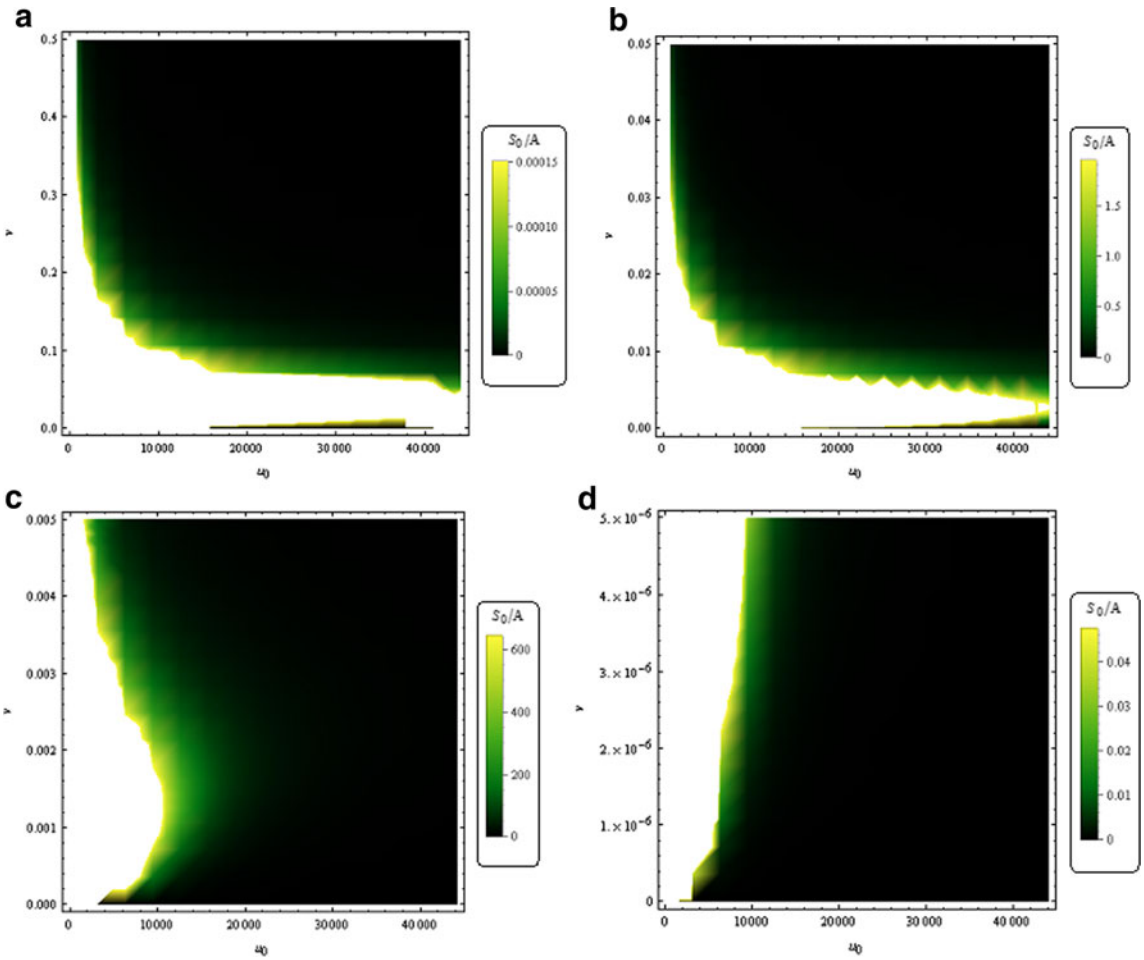

Fig. 5 Density plots of $\frac{S_0}{A}$ against v and u_0 for $D_0 = 2.19 \times 10^{-10} m^2 s^{-1}$, $p = -1$, $n = 0$. Different ranges of velocities are considered

We solve equation (4) by assuming that the solution is separable in the form

$$M_y(x,t) = C\psi(x)e^{\zeta t} \tag{5}$$

where t is the time between pulses. We apply the separation of variables technique to obtain an ordinary differential equation for the time- independent function ψ(x). Substituting equation (5) into equation (4) yields:

$$v^2\frac{d^2\psi(x)}{dx^2} + v(2\zeta + T_o)\frac{d\psi(x)}{dx} + \left(\zeta^2 + T_o\zeta + \gamma^2 B_1^2(x) + \frac{1}{T_1T_2}\right)\psi(x) = \frac{M_o\gamma B_1(x)}{T_1}e^{-\zeta t} \tag{6}$$

$$e^{\zeta t} \neq \frac{M_o\gamma B_1(x)}{v^2 T_1} \tag{7}$$

where ζ is any constant. RF $B_1(x)$ is the spatially varying magnetic field and v is the fluid flow velocity and $t = \left(\Delta - {}^{\delta}/_{3}\right)$. We apply a fundamental transformation procedure given as follows:

$$v = \frac{x}{\delta} \tag{8}$$

$$\gamma B_1(x) = \gamma g x \tag{9}$$

The assumptions are made that δ is infinitesimally short and negligible displacements occur those taking place during the pulse period compared with during the diffusion time, that is, $\delta << t$. In a typical MRI procedure, g is the pulsed gradient applied for the length of time t.

Substituting equations (9) into equation (6) gives

$$x^2\frac{d^2\psi(x)}{dx^2} + \delta(2\zeta + T_o)x\frac{d\psi(x)}{dx} + \left[\gamma^2 g^2\delta^2 x^2 + \delta^2\left(\zeta^2 + T_o\zeta + \frac{1}{T_1T_2}\right)\right]\psi(x) = \frac{M_o\delta^2\gamma B_1(x)e^{-\zeta t}}{T_1} \tag{10}$$

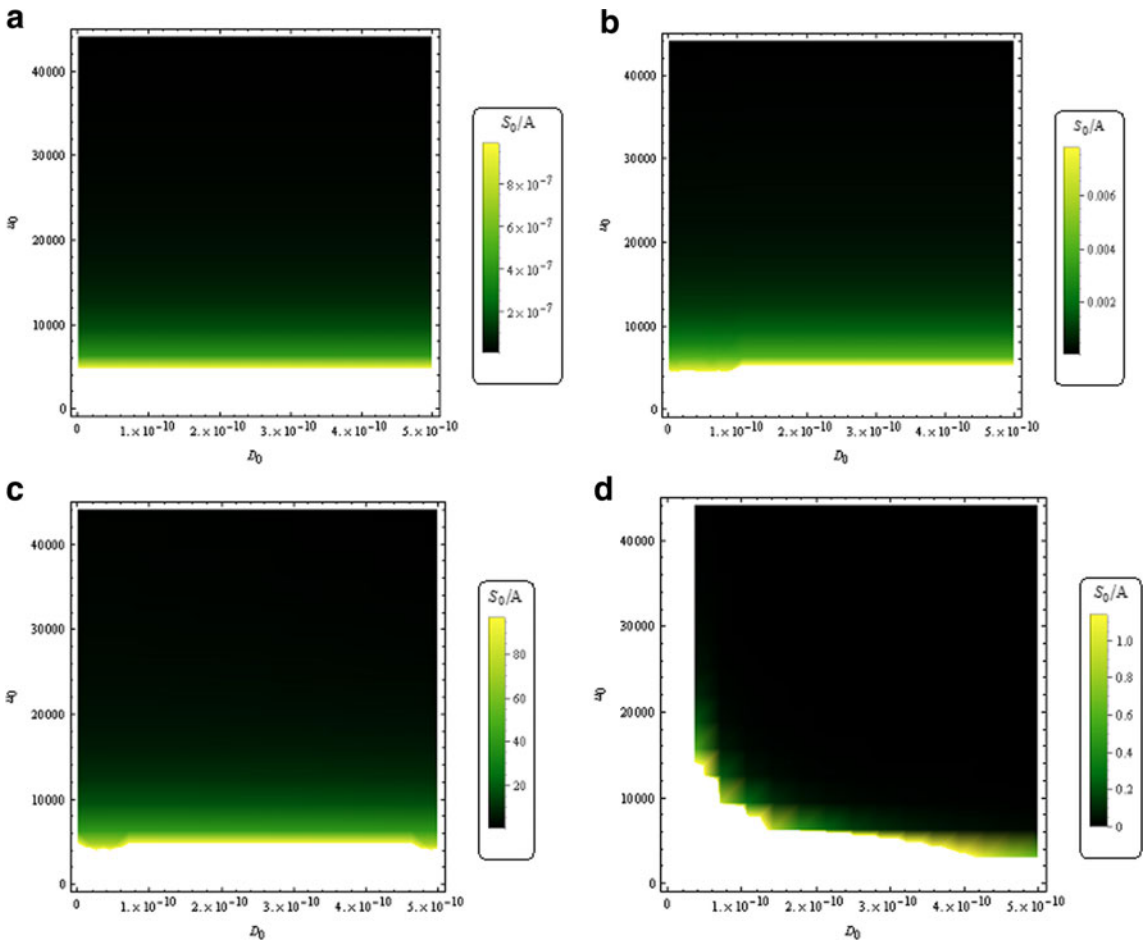

Fig. 6 Density plots of $\frac{S_0}{A}$ against v and u_0 for $D_0 = 2.19\times10^{-10}m^2s^{-1}$, $p = -1$, $n = 0$; (**a**) $v = 0.5ms^{-1}$ (**b**) $v = 0.05ms^{-1}$ (**c**) $v = 0.005ms^{-1}$ (**d**) $v = 5\mu ms^{-1}$

If the NMR is sampled at maximum magnitude (due to the application of maximum RF $B_1(x)$ field), $M_o \approx 0$. In this case, equation (10) becomes:

$$x^2\frac{d^2\psi(x)}{dx^2}+\delta(2\zeta+T_o)x\frac{d\psi(x)}{dx} + \left[\gamma^2g^2\delta^2x^2+\delta^2\left(\zeta^2+T_o\zeta+\frac{1}{T_1T_2}\right)\right]\psi(x)=0 \tag{11}$$

Equation (11) is transformable into Bessel's equation of order β and parameter $\gamma\delta g$ with general solution in the form:

$$\psi(x)=x^{-p}[AJ_n(u_0x)+A_1Y_n(u_0x)] \tag{12}$$

where u_o, η, β are all constants defined as:

$$n=\sqrt{p^2-\beta^2} \tag{13}$$

$$u_o=\gamma\delta g \tag{14}$$

$$\beta^2=\delta^2\left(\zeta^2+T_o\zeta+\frac{1}{T_1T_2}\right) \tag{15}$$

$$p=\frac{\delta(2\zeta+T_o)-1}{2} \tag{16}$$

$$T_0=\left(\frac{1}{T_1}+\frac{1}{T_2}\right)=\frac{(T_1+T_2)}{T_1T_2} \tag{17}$$

General behaviour of transverse magnetization

Since we always require that the transverse magnetization be finite as x tends to infinity, $A_1=0$. Therefore, the Stejskal and tanner formulation in equation (1) for diffusion NMR/MRI system in terms of Bessel function of the first kind where $\zeta=-u_0^2D_0$ is given by:

$$M_y(x,t)=Ax^{-p}J_n(u_0x)e^{-u_0^2D_0t} \tag{18}$$

$$\frac{M_y(x,t)}{A}=x^{-p}J_n(u_0x)e^{-u_0^2D_0t}=x^{-p}J_n(u_0x)e^{\zeta t} \tag{19}$$

where D_0 is the apparent diffusion coefficient (ADC) of the tissue. Using the relaxation times of some human tissues with carefully selected values of x and t, the curves crucial parameters of the solution in equation (19) are plotted; t = 20ms, δ = 20ms, g = 0.033Tm^{-1}, γ = 2.675 × 10^{8}s^{-1}T^{-1} [2, 27, 28] as shown in Table 1 and Fig. 1:We have varied time for the tissues in Table 1 and calculated the corresponding transverse magnetizations to make the plots in Figs. 2 and 3.

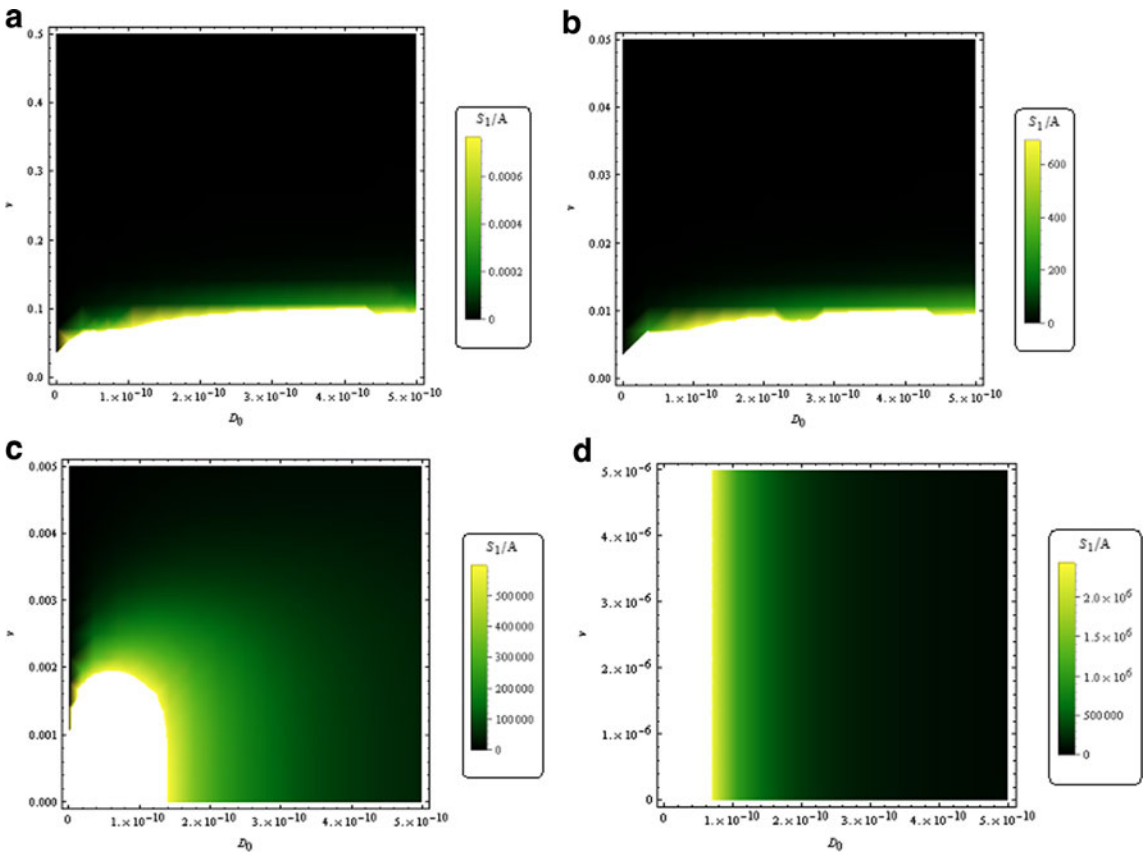

Fig. 7 Density plots of $\frac{S_1}{A}$ against v and D_0 for $u_0 = 44138\text{m}^{-1}$ (g = 33mTm^{-1}, δ = 20ms), $p = -1$, $n = 1$. Different ranges of velocities are considered

Direct NMR signal analysis

From equation (19), the expression of the NMR signal may be given as follows:

$$\frac{M_y(x,t)}{A} = J_n(u_0 x)e^{-u_0^2 D_0 t} \tag{20}$$

where

$$p = \frac{t(2\zeta + T_o) - 1}{2} = 0 \tag{21}$$

and

$$\frac{M_y(x,t)}{A} = xJ_n(u_0 x)e^{-u_0^2 D_0 t} \tag{22}$$

where

$$p = \frac{t(2\zeta + T_o) - 1}{2} = -1 \tag{23}$$

The signal based of equations (8, 18, 20) can be written as

$$\frac{S}{A} = \int_0^\infty vtJ_0(u_0 vt)e^{-u_0^2 D_0 t}dt = \frac{u_0 v^2}{\left(u_0^4 D_0^2 + u_0^2 v^4\right)^{3/2}} \tag{24}$$

For n = 0 and p = -1, and

$$\frac{S}{A} = \int_0^\infty vtJ_1(u_0 vt)e^{-u_0^2 D_0 t}dt = \frac{u_0^2 D_0}{\left(u_0^4 D_0^2 + u_0^2 v^4\right)^{3/2}} \tag{25}$$

For n = 1 and p = - 1.

The three dimensional plots of equations (24, 25) are shown in Figs. 4, 5, 6, 7, 8 and 9) with possible interesting applications under different NMR conditions based on the Bessel function of first kind with orders 0 and 1. Specifically, Figs. 5, 6, 8 and 9 show the significant influence of the parameter u_o on the NMR signal S (or the modified quantity S/A) and Figs. 7, 8, 9 indicate the important implications of changing the order of the Bessel function. Based on

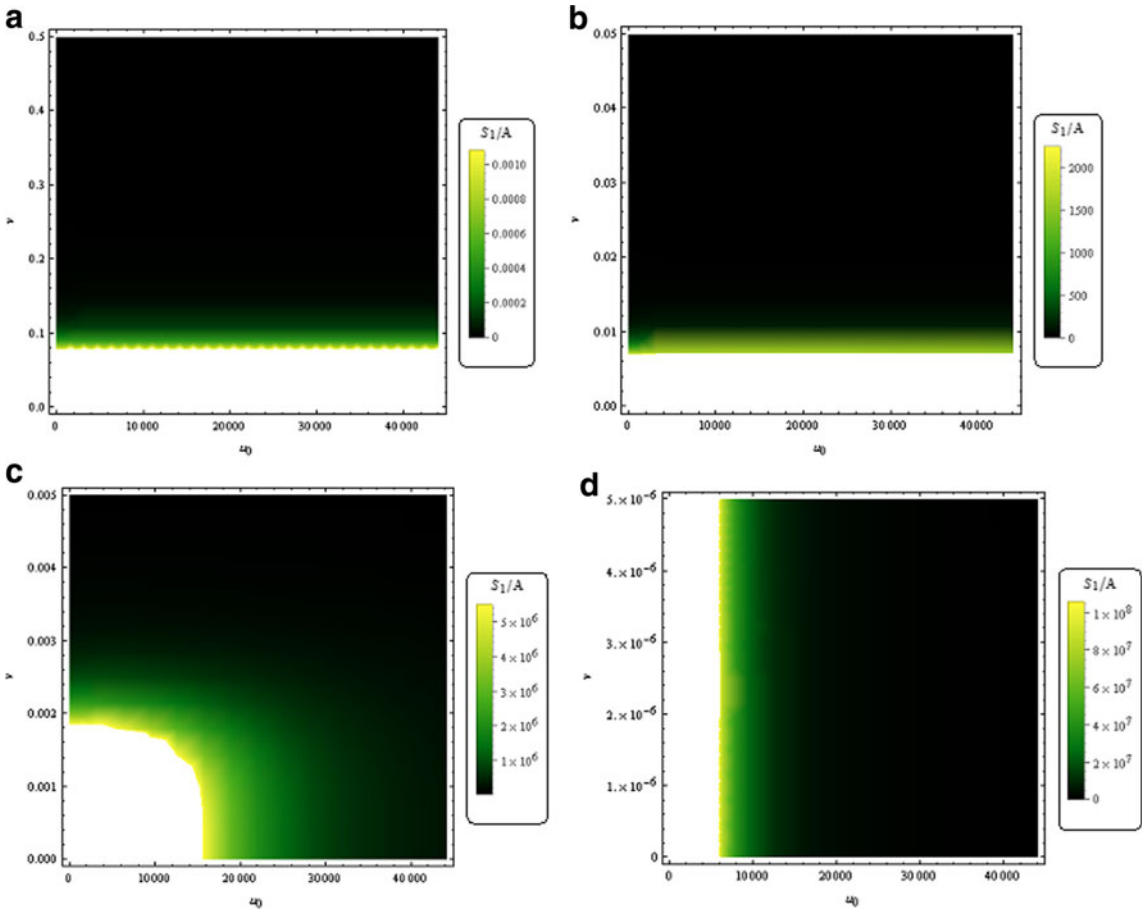

Fig. 8 Density plots of $\frac{S_1}{A}$ against v and u_0 for $D_0 = 2.19 \times 10^{-10} m^2 s^{-1}$, $p = -1$, $n = 1$. Different ranges of velocities are considered

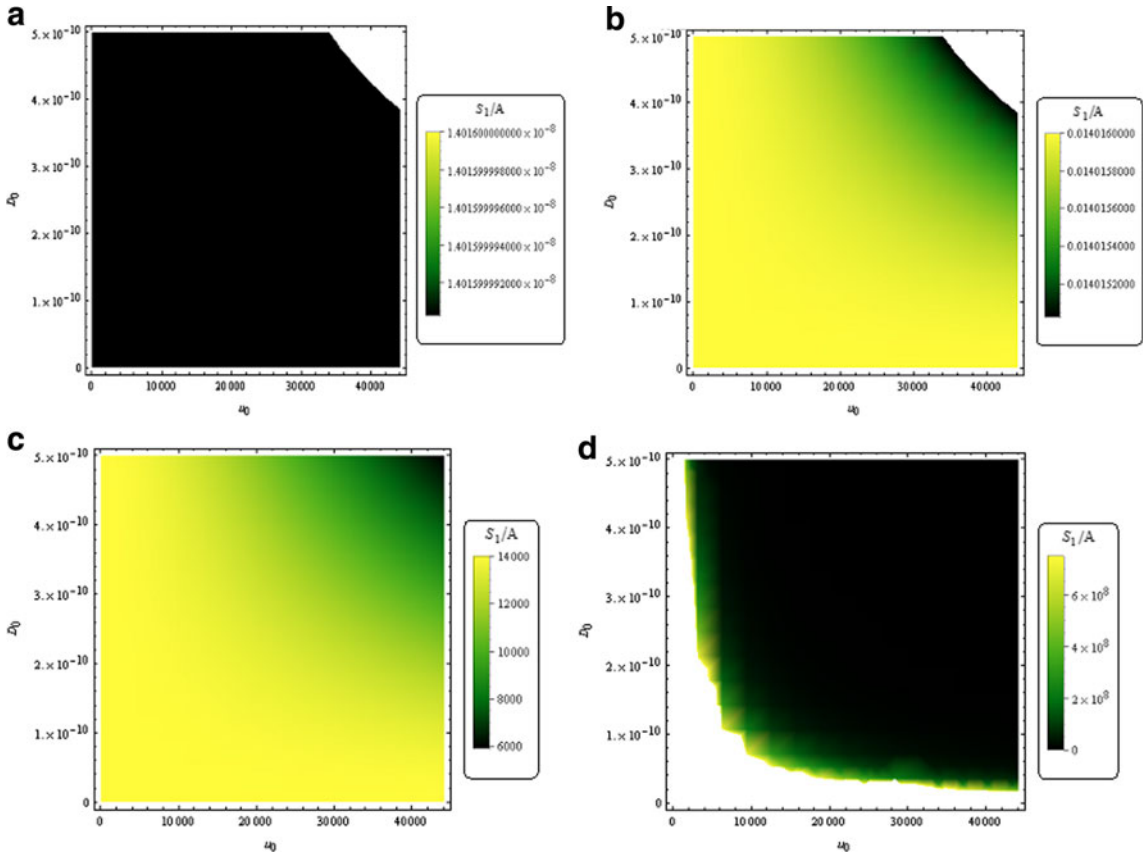

Fig. 9 Density plots of $\frac{S_1}{A}$ against v and u_0 for $D_0 = 2.19 \times 10^{-10} m^2 s^{-1}$, $p = -1$, $n = 1$; (**a**) $v = 0.5 ms^{-1}$ (**b**) $v = 0.05 ms^{-1}$ (**c**) $v = 0.005 ms^{-1}$ (**d**) $v = 5 \mu ms^{-1}$

equations (24, 25) and these figures, higher orders of Bessel function of the first kind can be very useful for the qualitative and quantitative analysis of complex flow. It is very interesting to note that the parameter n is very important in imaging different physiological flow processes. For $n = 0$, this model is very suitable to processes in which the velocities are in the millimeter range while at $n = 1$, best contrasts with high signal levels are obtained when the velocities are in the micrometer range. This may be very important in deciding on the method that is best for imaging the processes in the development and progression of human molecular diseases. However, we observed that at processes with nano-velocities, only the signal levels change slowly while the pattern and behaviour did not show any noticeable changes.

The detection system should be designed based on the Bessel function $J_n(u_0 x)$ which desribes the sensitivity of the receiver coil at different points in space therefore obeys equation (5). This is possible, because the basic objective of receiver coil design is to prescribe wire placements so that equation (12) has the largest possible transverse component [26]. Therefore, the time differentials of equations (24) and (25) are the values of the NMR signal for any given experimental constant n. This signal is the output voltage due to the induction of the nuclear magnetization $M_y(x,t)$. Thus, the sensitivity of the receiver coil is given by equation (12). If we take a point of reference as the longitudinal axis, it follows that $A_2 = 0$ since $Y_n(u_0 x)$ is unbounded as x approaches zero. Hence, for our design pirority, the sensitivity must be expressed as follows:

$$\psi(x) = AJ_n(u_0 x) \tag{31}$$

We shall assume that the receiver coil modifies the transverse magnetization $M_y(x,t)$ such that the arbitrary constant C_1 is taken as the receiver gain h, depending on the design of the receiver. Also, a phase shift φ, exists such that equation (31) takes the form:

$$\psi(\phi) = \frac{h}{\pi} \int_0^{\pi} \cos(n\phi - \phi \sin\phi) d\phi \tag{32}$$

where $n = 0, 1, 2, \ldots..$

In most biomedical applications, the voxel is very small and so is the value of x. Therefore, for $x << 1$, we write

$$\psi(\phi)|_n \approx \frac{1}{\Gamma(n+1)} \left(\frac{\phi}{2}\right)^n \tag{33}$$

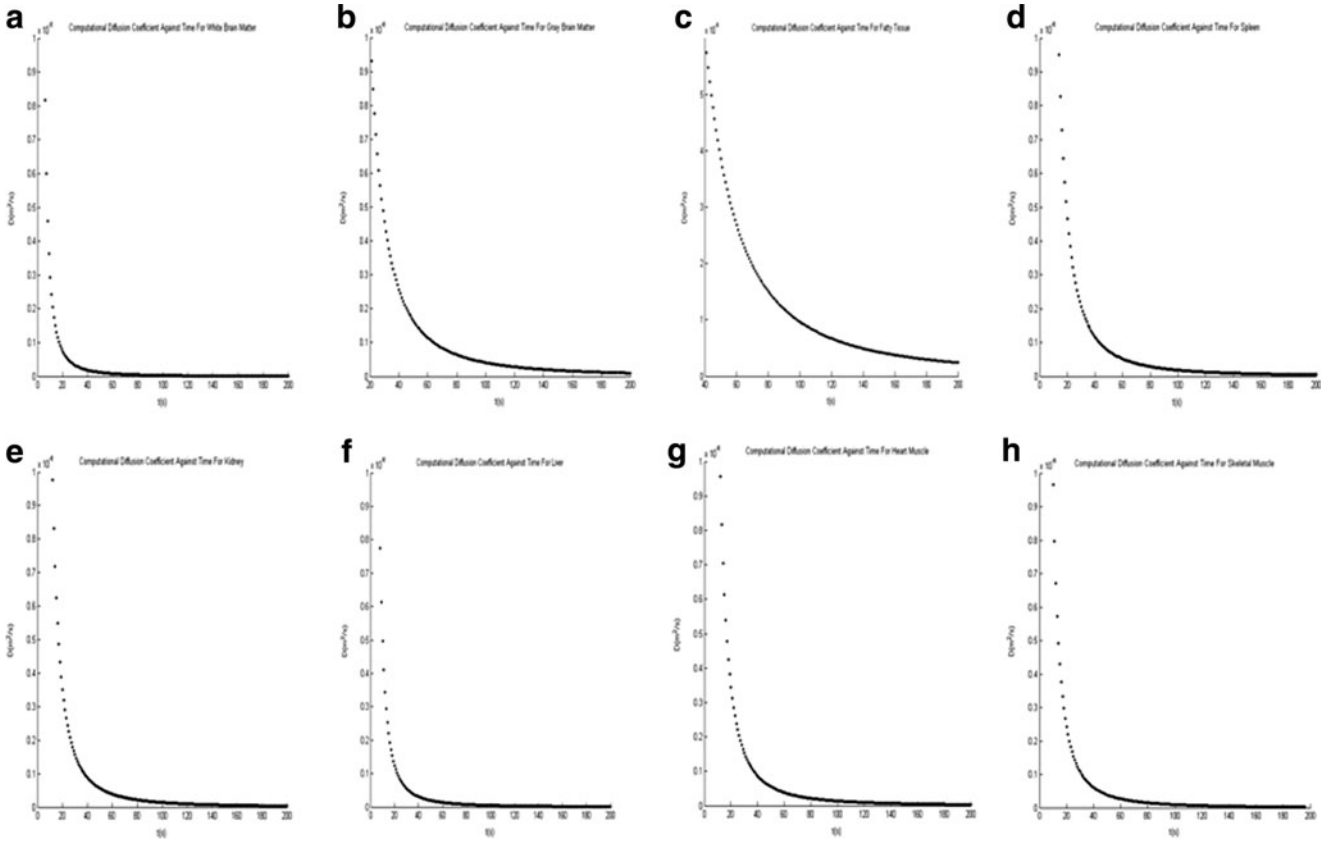

Fig. 10 Graph of computational diffusion coefficient against time for (**a**) white brain matter (**b**) gray brain matter (**c**) fatty tissue (**d**) spleen (**e**) kidney (**f**) heart muscle (**g**) skeletal muscle

where $\phi = u_0 x$ so that each property of Bessel function corresponds to a particular way of designing receiver coils for MRI experiments.

Computational analysis of diffusion coefficient

In this section we present data computed from equations (21) for some tissues experimental values of T_1, T_2, the magnetic gradient pulse g and the gyro-magnetic ratio of hydrogen γ. Figure 10 shows the natural behavior of diffusion with time in some selected biological tissues. This computational method can be applicable in numerous applications where diffusion analyses are involved.

For illustration, the diffusion of water molecules along a field gradient reduces the MR signal, the signal loss is less intense in areas of lower diffusion, and hence a brighter display is seen from this area as shown in Fig. 4. Diffusion weighting enables one to distinguish between rapid diffusion of protons (unrestricted diffusion) and slow diffusion of protons (restricted diffusion). The use of bipolar gradients pulses with any suitable pulse sequence permits the acquisition of diffusion weighted images. In a gradient echo (GE) Imaging Pulse Sequence, the bipolar gradient pulses as shown in Fig. 11a can be used directly. In the case of a spin echo pulse sequence, the diffusion weighting gradient pulses are positioned on either side of the 180 refocusing pulse and thus the gradient pulses will both be applied in the same direction based on the Bessel functions and properties as seen in Fig. 11b.

It may be informative to note that the MRI signals in equations (24) and (25) are velocity dependent. Since the fluid velocity is in the numerator of equation (24), extremely small values (such as those normally observed in molecular motion) leads to reduced values of the NMR signal while the absence of the velocity in the numerator of equation (25) leads to increased values of the signal for molecular flow velocity. However, for higher values of the fluid velocity (such as those observed in blood vessels), the signal calculated from equation (24) is considerably larger than that of equation (25). Hence, $n = 0$ is more suited for imaging physiological flows with large values of velocity while $n = 1$ is more suited for physiological flows in which the velocity is very small [29]. Based on equation (24–25) we have developed a computer program for physiological flows in ascending aorta, descending aorta, large arteries, capillaries, interstitial flow in tumour environment and membrane lipids [29–31] in Fig. 12.

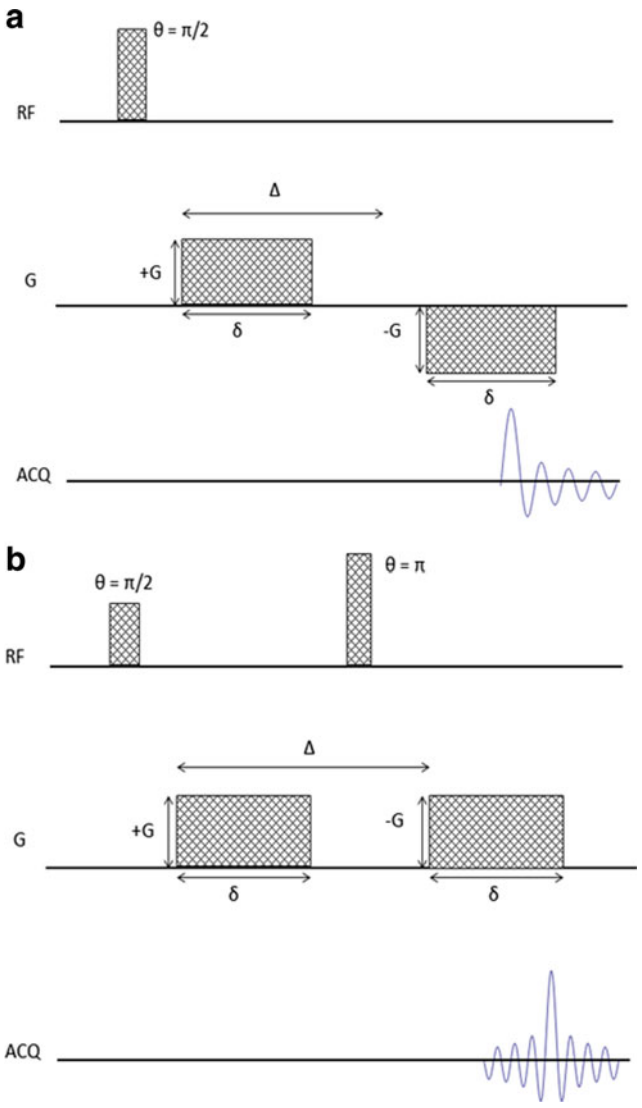

Fig. 11 A pulse sequence diagram of diffusion-weighted (**a**) gradient echo (GE) imaging pulse sequence (**b**) spin echo pulse sequence based on Bessel functions and properties

The physical interpretation of parameter n is apparent from equations (13), (15) and (16), where n is in term of NMR relaxation in the presence of diffusion. Parameter n is related to the pulse angle [32]; in the presence of flow and diffusion, we shall define a parameter called relaxation angle as given in equation (34) and Table 2.

$$\cos(\alpha_{dNMR}) = \exp(-n) = \exp\left(-\sqrt{\frac{(2\zeta\delta + \delta T_o - 1)^2}{4} - \delta^2\left(\zeta^2 + T_o\zeta + \frac{1}{T_1T_2}\right)}\right) \tag{34}$$

where α_{dNMR} is the relaxation angle in the presence of flow and diffusion. Based on table 3, the choice of pulse angle is critical for determining both signal intensity as well as image contrast. It also depends on the particular pulse sequence utilized.

Conclusion

Restricted flow was studied theoretically based on the time dependent Bloch flow equation [26]. A new analytical algorithm was developed for the NMR signal as a function of Bessel functions. This algorithm is shown to be very sensitive to highly complex or restricted flow at higher orders of Bessel functions. Based on our theoretical formulation, it is exciting to note that equations (22, 23) can be useful in characterizing restricted diffusion. The quantity ζ has been used extensively to explain the concept of restricted diffusion in the PFG NMR diffusion measurements [10]. In the case of freely diffusing particles, the diffusion coefficient determined by equation (1), will be independent of t. For short values of t in a restricted flow (such that the diffusing particle has not diffused far enough to feel the effect of the boundary), the measured diffusion coefficient will be the same as that observed, for the freely diffusing species. At very long t the maximum distance that the confined particle can travel is limited by the boundaries, and thus the measured mean-squared displacement and diffusion coefficient becomes independent of t. Thus, for short values of t, the measured displacement of a particle in a restricting flow observed via the signal attenuation in the PFG experiment is sensitive to the diffusion of the particle. At long t, the signal attenuation becomes sensitive to the shape and dimensions of the restricting flow [2]. Since nutrients are provided by direct diffusion from the circulatory system as a tumor grows the measured displacement of a cancerous cell in a restricting flow observed via the signal attenuation in the PFG experiment which is sensitive to diffusion can give pertinent information about the age, type, size and genesis of cancerous tissues. The advantage here is that ζ is obtained directly from the fundamental Bloch NMR flow equation without the need for the addition of arbitrary diffusion term.

Figures 1, 2 and 3 show how the NMR signal and flow velocity can be used to distinguish different tissues. This may offer new methods of distinguishing normal cells from cancerous cells based on Bessel properties and functions. More importantly, equation (18) defines the Bessel parameter u_o as a function of ζ used extensively in the earlier studies [2] to characterize diffusion in restricted geometries. The NMR/MRI detection system can always be desiged based on the Bessel functions with the appropriate choice of n and u_o. For illustration, most physiological processes are molecular in nature and the associated velocities are in micrometer range; showing that Figs. 7, 8 and 9) indicate that the human diseases can be detected at an early stage when $n > 0$.

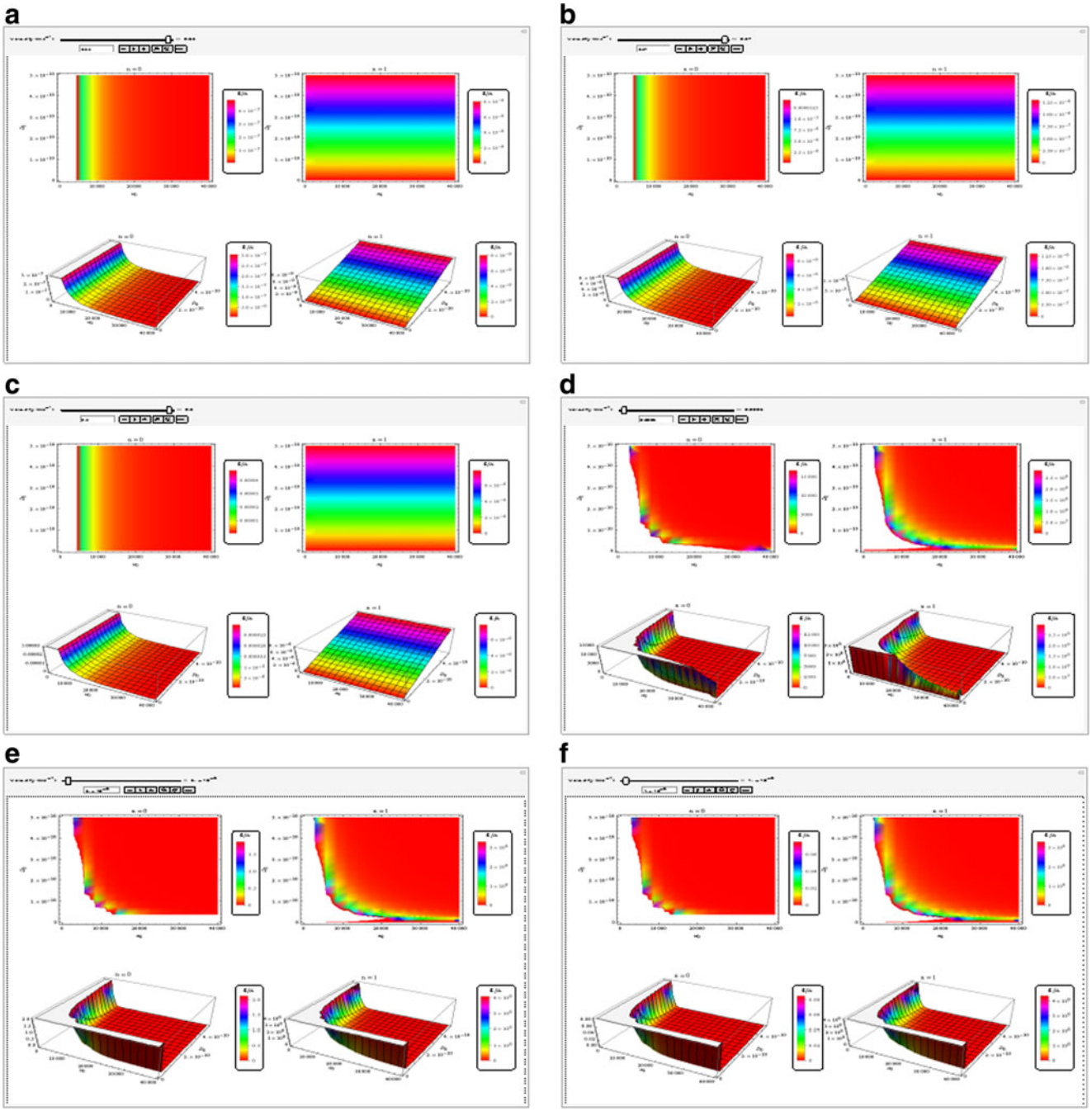

Fig. 12 Plots of the parameter S/A against u_0 and D_0 for (**a**) ascending aorta (0.63 m/s) (**b**) descending aorta (0.27 m/s) (**c**) large arteries (0.20 m/s) (**d**) capillaries (0.0005 m/s), (**g**) interstitial flow in tumour environment (5μm/s) and membrane lipids (1μm/s)

Figures 4, 5, 6, 7, 8 and 9) show the NMR/MRI signal based on Bessel functions and properties for the values of $n = 0$, 1 and $p = -1$ when the spin velocity assumes molecular values.

Equations (1, 2, 5, 24, and 25) reveal that the MRI signal S_o (in the absence of diffusion) obeys the Bessel functions and it is actually a function of diffusion coefficient as derived in this study. By varying the value of parameter u_o in the Bessel equation consequently changes the value of the pulse gradient as shown in Fig. 11. The MRI signal for any sample can be obtained uniquely based on the relaxation times as reflected in the value of n in equation (13).

What makes this algorithm unique and promising is that the NMR signal is based on the analytical solution of Bloch NMR flow equation using the well known

Table 2 The value of n in relation to the relaxation angle

n	exp (-n)	α_{dNMR} (rad)	α_{dNMR} (degrees)
0	1	0	0
0.25	0.778801	0.678045	38.849093
0.50	0.606531	0.919107	52.660932
0.75	0.472367	1.078822	61.811975
1.00	0.367879	1.194069	68.415104
1.25	0.286505	1.28022	73.351181
1.50	0.22313	1.345772	77.107051
2.00	0.135335	1.435044	82.221992
2.50	0.082085	1.488619	85.291578
3.00	0.049787	1.520989	87.146231
3.50	0.030197	1.540594	88.269554
4.00	0.018316	1.55248	88.950533
4.50	0.011109	1.559687	89.363488
5.00	0.006738	1.564058	89.613941
5.50	0.004087	1.56671	89.765845
6.00	0.002479	1.568318	89.857978
6.50	0.001503	1.569293	89.913859
7.00	0.000912	1.569884	89.947753
7.50	0.000553	1.570243	89.968311
8.00	0.000335	1.570461	89.980779
8.50	0.000203	1.570593	89.988342
9.00	0.000123	1.570673	89.992929
9.50	7.49E-05	1.570721	89.995711
10.00	4.54E-05	1.570751	89.997399
11.00	1.67E-05	1.57078	89.999043
12.00	6.14E-06	1.57079	89.999648
13.00	2.26E-06	1.570794	89.99987
14.00	8.32E-07	1.570795	89.999952
15.00	3.06E-07	1.570796	89.999982
15.50	1.86E-07	1.570796	89.999989
16.00	1.13E-07	1.570796	89.999994
16.50	6.83E-08	1.570796	89.999996
17.00	4.14E-08	1.570796	89.999998

Bessel functions. The advantage is that Bessel functions can be used for Diffusion weighted MRI by computational methods adapted for a particular experimental setting and medical need without acquiring sophisticated imaging facilities

Indeed, Bessel functions occur in many practical problems and very easy to be built into computer programs. In principle they are always to be expected when partial differential equations are used in the study of configurations involving circular geometries. On the other hand, they also arise in numerous applications where neither circular symmetry nor partial differential equations are involved. This makes the algorithm presented here to be versatile and applicable in a variety of problems. Specifically, the sensitivity of the NMR/MRI system can be explicitly controlled by the order n of the Bessel function with parameter u_o. This can be simple and easy to manipulate as situation requires and can be very useful in most NMR/MRI experimental settings.

Acknowledgments The correspondence author acknowledges the supports of Prof. M.A. Akanji, Vice Chancellor, Federal University of Technology, Minna, Nigeria and Prof. A.G. Ambali, Vice Chancellor, University of Ilorin, Ilorin, Nigeria in facilitating sabbatical leave for one of the authors which provide improved academic environment that enhance the quality of this work. The supports of Swedish International Development Agency (SIDA) through the Abdus Salam International Centre for Theoretical Physics (ICTP), Trieste, Italy and Dr. K.J. Oyewumi, Head, Department of Physics, University of Ilorin are equally acknowledged.

References

1. Magnetic Resonance Angiography. Wikipedia: The Free Encyclopedia. https://en.wikipedia.org/wiki/Magnetic_resonance_angiography. Accessed 12 June 2014.
2. Price, W. S., Pulsed field gradient nuclear magnetic resonance as a tool for studying translational diffusion: part I. basic theory. *Concepts. Magn. Reson.* 9:299–336, 1997.
3. Tanner, J. E., Transient diffusion in system partitioned by permeable barriers. application to NMR measurements with a pulsed field gradient. *J. Chem. Phys.* 69(4):1748–1754, 1978.
4. Price, W. S., and Kuchel, P. W., Effect of nonrectangular field gradient pulses in the Stejskal and Tanner (diffusion) pulse sequence. *J. Magn. Reson.* 94:133–139, 1991.
5. Taylor, D. G., and Bushell, M. C., The spatial mapping of translational diffusion coefficients by the NMR imaging technique. *Phys. Med. Biol.* 30(4):345–349, 1985.
6. Chang, D. C., Hazlewood, C. F., Nichols, B. L., and Rorschach, H. E., Spin echo studies on cellular water. *Nature* 235(5334):170–171, 1972.
7. Chang, D. C., Rorschach, H. E., Nichols, B. L., and Hazlewood, C. F., Implications of diffusion coefficient measurements for the structure of cellular water. *Ann. NY Acad. Sci.* 204:434–443, 1973.
8. Rorschach, H. E., Chang, D. C., Hazlewood, C. F., and Nichols, B. L., The diffusion of water in striated muscle. *Ann. NY Acad. Sci.* 204(1):444–452, 1973.
9. Cooper, R. L., Chang, D. B., Young, A. C., Martin, C. J., and Ancker-Johnson, B., Restricted diffusion in biophysical systems. *Exp. Biophys. J.* 14(3):161–177, 1974.
10. Hazlewood, C. F., Rorschach, H. E., and Lin, C., Diffusion of water in tissues and MRI. *Magn. Reson. Med.* 19(2):214–216, 1991.
11. Awojoyogbe, O. B., Dada, O. M., Faromika, O. P., and Dada, O. E., Mathematical concept of the Bloch flow equations for general magnetic resonance imaging: a review. *Concepts Magn. Reson. A* 38(3): 85–101, 2011.
12. Awojoyogbe, O. B., Karim, B., Aweda, M. A., and Dada, M., BPES-related mathematical development for the phase shift due to Rf magnetic field in heart inferior coronary artery NMR imaging. *J. Clin. Experiment Cardiol.* 1:111, 2010.
13. Awojoyogbe, O. B., and Dada, M., Basis for the applications of analytical models of the bloch NMR flow equations for Functional Magnetic Resonance Imaging (fMRI): a review. *Recent Pat. Med. Imag.* 2:22–56, 2011.
14. Awojoyogbe, O. B., and Dada, M., The dynamics of NMR-diffusion equation for the analysis of hemodynamic and metabolic

changes in biological tissue. In: Berg, E. T. (Ed.), *Fluid Transport: Theory, Dynamics and Applications*. Nova, New York, pp. 183–217, 2011.

15. Sim, K. S., Lai, M. A., Tso, C. P., and Teo C. C. Single image signal-to-noise ratio estimation for magnetic resonance images. *J. Med. Syst.* 35(1):39–48.
16. Daliri, MR. Automated diagnosis of Alzheimer disease using the scale-invariant feature transforms in magnetic resonance images. *J. Med. Syst.* 36(2):995–1000.
17. Awojoyogbe, O. B., Faromika, O. P., Moses, F. O., Dada, M., Boubaker, K., and Fuwape, I. A., Mathematical model of the Bloch NMR flow equations for the analysis of fluid flow in restricted geometries using the Boubaker polynomials expansion scheme. *Curr. Appl. Phys.* 10(1):289–93, 2010.
18. Dada, M., Awojoyogbe, O. B., Moses, O. F., Ojambati, O. S., and De, D. K., A mathematical analysis of Stenosis Geometry, NMR magnetizations and signals based on the Bloch NMR flow equations, Bessel and Boubaker polynomial expansions. *J. Biol. Phys. Chem.* 9(3):101–106, 2009.
19. Awojoyogbe, O. B., Faromika, O. P., Dada, M., Boubaker, K., and Ojambati, O. S., Mathematical models of real geometrical factors in restricted blood vessels for the analysis of CAD (coronary artery diseases) using legendre, Boubaker and Bessel polynomials. *J. Med. Syst.* 35(6):1513–20, 2011.
20. Dada, M., Awojoyogbe, O. B., Boubaker, K., and Ojambati, O. S., BPES analyses of a new diffusion-advection equation for fluid flow in blood vessels under different bio-physico-geometrical conditions. *J. Biophys. Struct. Biol.* 2(3):28–34, 2010.
21. Awojoyogbe, O. B., and Boubaker, K., A solution to Bloch NMR flow equations for the analysis of hemodynamic functions of blood flow system using m-Boubaker polynomials. *Curr. Appl.* 9(1):278–283, 2008.
22. Awojoyogbe, O. B., A quantum mechanical model of the Bloch NMR flow equations for electron dynamics in fluids at the molecular level. *Phys. Scr.* 75:788–794, 2007.
23. Awojoyogbe, O. B., A mathematical model of Bloch NMR equations for quantitative analysis of blood flow in blood vessels with changing cross-section I. *Phys. A* 303(1):163–175, 2002.
24. Awojoyogbe, O. B., A mathematical model of Bloch NMR equations for quantitative analysis of blood flow in blood vessels with changing cross-section II. *Phys. A* 323:534–550, 2003.
25. Awojoyogbe, O. B., Analytical solution of the time dependent Bloch NMR equations: a translational mechanical approach. *Phys. A* 339:437–460, 2004.
26. Hinshaw, W. S., and Lent, A. H., An introduction to NMR imaging: from the Bloch equation to the imaging equation. *Proc. IEEE* 71(3): 338–50, 1983.
27. Harris, R. K., *Nuclear Magnetic Resonance Spectroscopy.* Wiley, New York, 1986.
28. Brix, G., Kolem, H., Nitz, W. R., Bock, M., Huppertz, A., Zech, C. J., and Dietrich, O., Basics of magnetic resonance imaging and magnetic resonance spectroscopy. In: Reiser, M. F., Semmler, W., Hricak, H., and Hrsg (Eds.), *Magnetic Resonance Tomography.* Springer, Berlin, pp. 3–167, 2008.
29. Nelson, D. L., Lehninger, A. L., and Cox, M. M., *Lehninger Principles of Biochemistry.* Macmillan, United Kingdom, p. 42, 2008.
30. Galdi, G. P, Rannacher, R., Robertson, A. M., and Turek, S. (2008)., Hemodynamical Flows: Modeling, Analysis and Simulation. In Oberwolfach Seminars (37). Basel: Birkhäuser Verlag AG.
31. Tung, C. K., Krupa, O., Apaydin, E., Liou, J. J., Diaz-Santana, A., Kim, B. J., and Wu, M., A contact line pinning based microfluidic platform for modelling physiological flows. *Lab Chip* 13(19): 3876–3885, 2013.
32. Haacke, E. M., Brown, R. W., Thompson, M. R., and Venkatesan, R., *Magnetic Resonance Imaging: Physical Principles and Sequence Design*. Wiley, New York, 1999.